Reaction Kinetics, Mechanisms and Catalysis (2022) 135:1099–1111
https://doi.org/10.1007/s11144-022-02187-w

Synthesis of $C_{60}/Cd_{0.5}Zn_{0.5}S$ nanocomposite with high photocatalytic activity for the degradation of Rhodamine B

Hewei Zhang[1] · Congcong Duan[1] · Zhen Xu[1] · Jiahang Yin[1]

Received: 20 December 2021 / Accepted: 13 February 2022 / Published online: 23 February 2022

Abstract

Herein, the $C_{60}/Cd_{0.5}Zn_{0.5}S$ (C_{60}/CZS) photocatalysts with excellent photocatalytic performance were prepared using facile one-pot hydrothermal method. The crystal structure, morphology, photoelectric performance and photocatalytic activity of the samples were characterized by XRD, XPS, UV–Vis and electrochemistry. The catalytic degradation of pollutants under the irradiation of visible light was simulated using Rhodamine B (Rh B). The content of C_{60} was changed from 0.5 to 5 wt%, and the optimal value for the photocatalytic activity was determined to be 2 wt%. The apparent degradation rate and degradation efficiency of Rh B were 0.024 min^{-1} and 97.5% within 140 min, which is 3.4 times that of pure CZS. C_{60}/CZS exhibited excellent catalytic performance, and its photocatalytic activity was sustained even after three cycles. Moreover, electrochemical test results demonstrated that the separation and transfer of photocarriers on CZS surface were effectively improved by C_{60}, thus enhancing its activity. In this study, we innovatively prepared a novel photocatalyst by combining fullerenes with sulfide solid solution for the first time, which has rarely been studied in the past. The synthetic method is simple, efficient and pollution-free. Subsequently, the catalytic degradation of Rh B experiment confirmed that the catalyst has high catalytic efficiency and stability. This experiment has practical significance not only for the catalytic degradation of Rh B but also for the application of fullerene in photocatalysis.

Keywords Fullerene (C_{60}) · Chalcogens · Rhodamine B · Nanocomposite · Photochemistry

✉ Hewei Zhang
hewei97015@163.com

[1] State Key Laboratory of Advanced Technology for Materials Synthesis and Processing, Wuhan University of Technology, Wuhan 430070, China

Introduction

Rapid developments in technology have greatly improved people's lives. However, environmental pollution has emerged as a serious global concern. For decades, numerous efforts have been made on environmental remediation [1, 2]. Several solutions have emerged from scientific efforts, among which photocatalysis is very simple, cheap, with the ability to use solar energy directly [3]. There are many efficient photocatalysts, among which cadmium sulfide (CdS) is widely explored with a suitable band gap of 2.45 eV and coincides with the visible region of sunlight [4–6]. There are two critical disadvantages that limit the further application of CdS photocatalysts—a high photogenerated electron–hole pair recombination rate and photocorrosion problem [7–9].

The CdZnS solid solutions consisting of narrow-bandgap CdS and wide-bandgap ZnS are effective in solving the aforementioned concerns [10, 11]. As a typical alloy sulfide semiconductor, a CdZnS solid solution photocatalyst reacts to visible light and have a greater negative conduction band (CB) position and corrected valence band (VB) position [12, 13]. In addition, the ratio of Cd to Zn regulates the band structure [14, 15]. Tang et al. [16] used cadmium, zinc, and thiourea as precursors and PVP as a surfactant to obtain CdZnS nanospheres by a hydrothermal method at 150 °C. Numerous experiments have been conducted to confirm that when the proportion of Cd and Zn is equal, $Cd_{0.5}Zn_{0.5}S$ shows the best catalytic performance [17–19]. However, the photocatalytic efficiency of $Zn_xCd_{1-x}S$ can still be improved. Doping with other substances is generally considered to be an efficient method to achieve the same outcome [20, 21]. The heterojunction structure inhibits the photoinduced electron–hole recombination probability and improves the catalytic efficiency effectively.

Fullerene (C_{60}), composed of 60 carbon atoms, is the third allotrope of carbon. It is a football-like nanomolecule with a 32-hedron structure, 0.7 nm molecular diameter, and 1 nm van der Waals diameter. Its lowest unoccupied molecular orbital energy is low, and it can reversibly accept one to six electrons in the solid and solution [22, 23]. Therefore, C_{60} can be used as an electron library for absorbing and releasing electrons and has a rich chemical reactivity. In addition, the highly symmetric large π-conjugated bond system and conical arrangement of carbon atoms enable C_{60} to effectively separate photogenerated charges and recombine charges relatively slowly during electron transport [24–26]. Hence, C_{60}, as a potential photosensitive material, can be compounded with semiconductor photocatalytic materials to improve the separation and migration of photogenerated charges, thereby enhancing the photocatalytic activity. Using the Bi_2WO_6 photocatalyst modified by C_{60}, it was found that the Rhodamine B (Rh B) and MB dyes have high degradation efficiency under visible light and sunlight and focus on the synergistic effect [27]. The synthesized complex using a hydrothermal method showed a greater degradation efficiency than pure TiO_2 under visible light, and studied different photocatalytic mechanisms under different light sources [28]. Thus, C_{60} enhanced Zn–Cd matrix composites have high photocatalytic activity and stability, which has a huge market demand.

Herein, we report a facile one-pot hydrothermal preparation method for a C_{60}/$Cd_{0.5}Zn_{0.5}S$ nanocomposite and study its photocatalytic performance under visible light irradiation, where the quantity of C_{60} varied from 0.5 to 5 wt% (0.5%, 1%, 2%, and 5%), and the optimal value for photocatalytic activity was proved to be 2 wt%. This novel C_{60}/$Cd_{0.5}Zn_{0.5}S$ nanocomposite exhibits immense potential for environmental modification.

Experimental

Materials

$Cd(CH_3COO)_2.2H_2O$, $Zn(CH_3COO)_2$, CH_4N_2S, and C_{60} were got from Aladdin Reagent Company (Shanghai, China). Deionized (DI) water used here was obtained from laboratories.

Preparation of C_{60}/$Cd_{0.5}Zn_{0.5}S$ nanocomposites

The first acidizing treatment of C_{60} was implemented before synthesizing nanocomposites for higher dispersity. First, 100 mg raw C_{60} was evenly mixed in 40 mL of mixed acid (H_2SO_4:HNO_3 = 3:1) and dispersed for a period of time at room temperature. It was then placed in a three-necked bottle for stirring and acidification at 60 °C for 4 h. Finally, it was diluted and washed by DI water several times until the pH was 7. The product was then placed back into the oven for drying, so as to obtain acidified C_{60}.

C_{60}/$Cd_{0.5}Zn_{0.5}S$ nanocomposites were synthesized via the hydrothermal reaction. Subsequently, 3 mmol of $Cd(CH_3COO)_2{\cdot}2H_2O$, 3 mmol of $Zn(CH_3COO)_2$, 7 mmol of CH_4N_2S, and C_{60} dissolved in 60 mL of deionized water and were vigorously stirred for 30 min. Then, a homogeneous suspension was created and moved to a high-temperature and high-pressure reaction kettle and kept at 180 °C for 12 h. The autoclave was then dropped to indoor temperature. The yellow precipitate was centrifugally many times and then maintained in a 70 °C vacuum oven for 24 h. The weight percentage of C_{60} was set as 0.5%, 1%, 2%, and 5% to explore its effect on the photocatalytic activity of C_{60}/$Cd_{0.5}Zn_{0.5}S$ nanocomposites. The obtained samples were labelled as $0.5C_{60}$/CZS, $1C_{60}$/CZS, $2C_{60}$/CZS, and $5C_{60}$/CZS.

Characterization

The patterns of X-ray diffraction (XRD) and the UV–Vis absorption spectrum were obtained by a Palmer naco diffractometer (Empyrean, Netherlands) with Cu K_α radiation and a UV–Vis spectrophotometer (Lambda 750S, USA). The Fourier transform infrared (FT-IR) spectra and X-ray photoelectron spectroscopy (XPS) were measured using a Nexus FT-IR spectrometer, and an ESCALAB 250Xi X-ray photoelectron spectrometer. The Brunauer–Emmett–Teller (BET) surface area was determined by a multipoint BET method using adsorption data in the relative pressure (P/

P_0) range of 0.05–0.3. The CHI 660 B electrochemical system (Shanghai, China) was applied to carry out electrochemical impedance spectroscopy (EIS) and photocurrent measurements with a standard three-electrode cell system.

Photocatalytic degradation of Rh B

Through the Rh B aqueous solution degradation under the irradiation of visible light, the photocatalytic activities of the $C_{60}/Cd_{0.5}Zn_{0.5}S$ nanocomposites (or $Cd_{0.5}Zn_{0.5}S$ reference) were determined. To be specific, the photocatalyst prepared by 30 mg was ultrasonic dispersed in 60 mL of Rh B solution (10 mg/L), which was maintained with a 300 W xenon lamp and a 420 nm cut-off filter offering visible light. The suspension was magnetized and stirred for 30 min in the dark to obtain the adsorption–desorption balance, before the lamp was turned on. After a certain period of irradiation, an appropriate amount of reaction solution was collected, while the photocatalyst and Rh B solution were separated through vacuum suction filtration. Rh B solution concentration was measured using with the 554 nm absorbance UV–Vis spectrometer. The photocatalytic degradation of each sample follows the non-linear least squares fitting equation:

$$A = C \times \exp(-k \times t) + E$$

A is the amplitude of the process, C is the concentration of reactant after degradation of Rh B, E is the end point, and k is the degradation rate constant[29].

Results and discussion

XRD characterization

The XRD pattern of the C_{60}/CZS nanocomposites with different C_{60} composition ratios were shown in Fig. 1a. The diffraction peaks at 24.8°, 26.5°, 28.2°, 36.6°, 43.7°, 47.8°, and 52.8° correspond to the (100), (002), (101), (102), (110), (103), and (201) crystal surfaces of $Cd_{0.5}Zn_{0.5}S$. This is consistent with the standard card (JCPDS No. 49-1302), indicating that the synthesis of hexagonal $Cd_{0.5}Zn_{0.5}S$ is successful. In addition, the pattern showed no change after the introduction of C_{60}, indicating that its introduction did not change the crystal structure of CZS. Fig. 1b presents a partially enlarged view of the XRD patterns from 10° to 22°. The content of C_{60} is low ($\leq$1 wt%), and the diffraction peak is not obvious. However, three peaks at 10.8° (111), 17.7° (200), and 20.8° (311) were obtained with 2 wt% C_{60}. It can be labeled as the cubic phase of C_{60} (JCPDS No. 44-0558), confirming that C_{60}/CZS was synthesized.

XPS profiles

X-ray photoelectron spectroscopy profiles were recorded to explore the chemical properties of C_{60}/CZS nanocomposites. XPS measurements were used to research

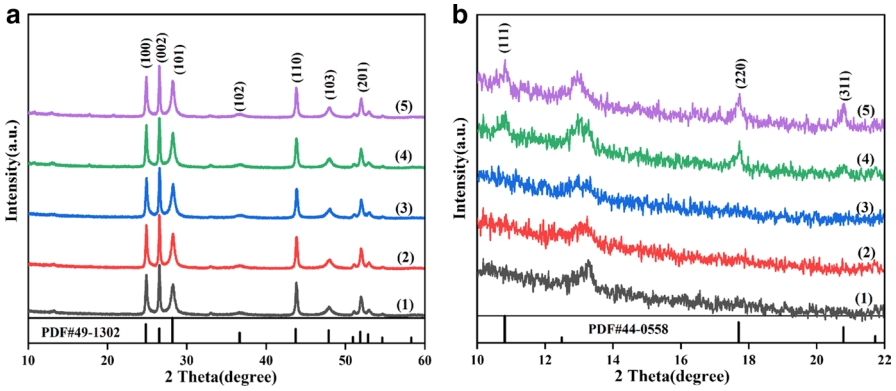

Fig. 1 **a** X-ray diffractometer pattern of CZS, $0.5C_{60}$/CZS, $1C_{60}$/CZS, $2C_{60}$/CZS, and $5C_{60}$/CZS(XRD condition: Empyrean, 10°–60°, 10°/min) **b** local X-ray diffractometer pattern of CZS, $0.5C_{60}$/CZS, $1C_{60}$/CZS, $2C_{60}$/CZS, and $5C_{60}$/CZS from 10° to 22° (1) $Cd_{0.5}Zn_{0.5}S$; (2) $0.5C_{60}$/CZS; (3) $1C_{60}$/CZS; (4) $2C_{60}$/CZS; (5) $5C_{60}$/CZS

the chemical state of the constituent elements and chemical composition of $2C_{60}$/CZS nanocomposites (Fig. 2). The XPS survey spectrum results demonstrated that the sample contained C, S, Cd, and Zn (Fig. 2a). The peaks of C1s appeared at 284.3 eV, 286.0 eV and 289.3 eV, among which the peak at 284.3 eV belongs to the adventitious carbon and C_{60} (Fig. 2b). The peak at 286.0 eV is portioned to the oxidized C–O, as produced by oxidizing the defective sp^{2-} hybridized C_{60}. Furthermore, the peak at 289.3 eV was supposed to be caused from carboxyl carbon (C = C–O) [30]. Fig. 2c and d show the XPS profiles of the Cd 3d and Zn 2p orbitals, respectively, with the binding energies of the Cd 3d orbital are at 406.0 eV, 411.3 eV and the Zn 2p at 1021.8 eV, 1044.9 eV, distinctly different from those for pure ZnS and CdS combination on the corresponding orbit. Therefore, it was concluded that the prepared catalyst was a metal complex sulfide, not pure ZnS and CdS mixture. Additionally, the interaction between metals caused differences in the binding energy. As suggested by the S 2p peaks at 161.0 eV and 162.2 eV, the common form of existing S in $Cd_{0.5}Zn_{0.5}S$ is S^{2-} (Fig. 2e).

UV–Vis diffuse reflectance spectrum

The UV–Vis spectra for different ratios in the C_{60}/CZS composite were determined (Fig. 3a). The absorption band edge of CZS is at 490 nm, which is consistent with its direct bandgap (2.4 eV). Consequently, visible light can be directly used for the catalytic reaction. Compared with pure CZS, the absorption band edge of each C_{60}/CZS sample shows barely any change, indicating that the carbon atoms in C_{60} do not enter the lattice of CZS and are bonded only by physical adsorption. In addition, the bandgap width of each C_{60}/CdS sample as calculated using the Kubelka–Munk [31] method is almost equal to that of pure CZS (Fig. 3b), indicating that the introduction of C_{60} will not affect the bandgap width of CZS but only slightly enhance the light absorption ability.

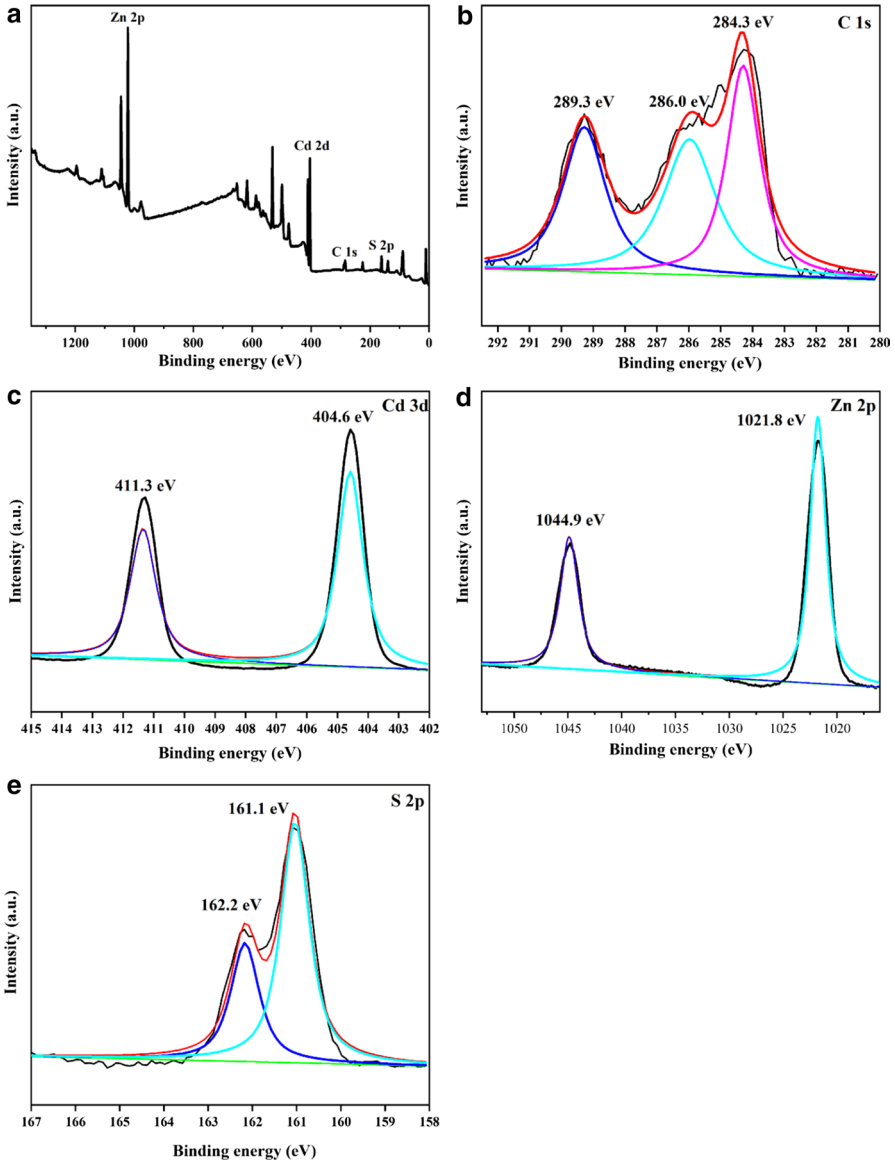

Fig. 2 X-ray photoelectron spectroscopy survey spectrum of $2C_{60}$/CZS: **a** survey; **b** C 1 s; **c** Cd 3d; **d** Zn 2p; and **e** S 2p (XPS condition: ESCALAB 250Xi; the contaminant carbon(C1s = 284.6 eV) was chosen as a reference for calibration of the binding energies)

Photocatalytic activity and stability

The photocatalytic degradation of Rh B under visible light irradiation was explored and the photocatalytic reaction of the as-obtained samples was determined. Degradation efficiency of the C_{60}/CZS photocatalysts with various C_{60} mass ratios

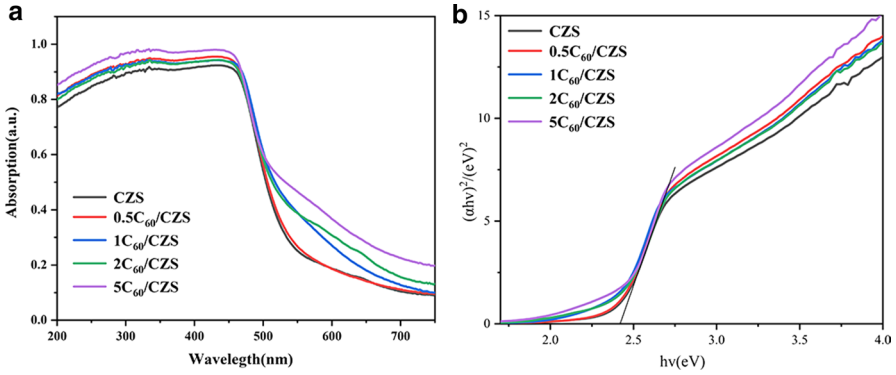

Fig. 3 **a** Ultraviolet visible diffuse reflectance spectra of CZS, $0.5C_{60}$/CZS, $1C_{60}$/CZS, $2C_{60}$/CZS, and $5C_{60}$/CZS **b** band gap width of CZS, $0.5C_{60}$/CZS, $1C_{60}$/CZS, $2C_{60}$/CZS, and $5C_{60}$/CZS(UV–Vis diffusion spectroscopy condition: Lambda 750 S, Wavelength range: 200–750 nm, Absorption ratio reference: $BaSO_4$; Eg calculation formula: $[(\alpha h\nu)^{1/n} = A(h\nu - E_g)]$, n = 1/2)

were shown in Fig. 4a presents. In the adsorption stage, the decolorization rates of $Cd_{0.5}Zn_{0.5}S$, $0.5C_{60}$/CZS, $1C_{60}$/CZS, $2C_{60}$/CZS, and $5C_{60}$/CZS to Rh B are 15.4%, 17.2%, 23.2%, 24%, and 22%. The adsorption rate of C_{60}/CZS is slightly higher than that of CZS. This may be because C_{60}/CZS has a slightly larger surface area than CZS. During the photocatalysis, the degradation rates of all C_{60}/CZS catalysts for Rh B were much higher compared with pure $Cd_{0.5}Zn_{0.5}S$. Additionally, the photocatalytic degradation rate of $2C_{60}$/CZS for Rh B was the highest, reaching 97.5%. In comparison, it was 61% for pure $Cd_{0.5}Zn_{0.5}S$, 86.3% for $0.5C_{60}$/CZS, 89.5% for $1C_{60}$/CZS, and 93% for $5C_{60}$/CZS. Thus, it can be confirmed that 2 wt% was the optimum.

The entire photocatalytic degradation process conforms to non-linear least squares fitting equation [32]. The rate constant (k), standard deviation (σ) and

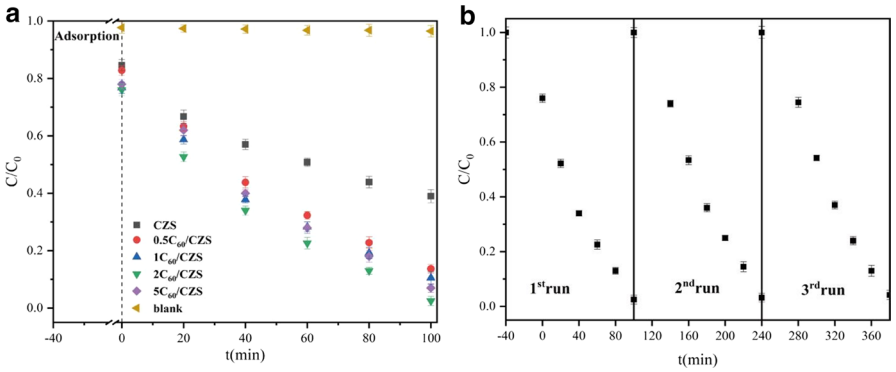

Fig. 4 **a** Photocatalytic degradation of RhB by CZS, $0.5C_{60}$/CZS, $1C_{60}$/CZS, $2C_{60}$/CZS, and $5C_{60}$/CZS. **b** Recycling experiments of visible-light photocatalytic degradation of RhB over the $2C_{60}$/CZS(experimental conditions: $[Rh\ B]_0 = 10$ mg/L, catalyst dose = 30 mg, vsolution = 60 mL, 300 W xenon lamp, λ > 420 nm, illumination time: 100 min)

Table 1 The standard deviation (σ) for photocatalytic degradation RhB with correlation coefficient value (R^2) and the rate constants by the non-linear least squares fitting

Sample	k (min^{-1})	σ	R^2
CZS	0.007	7×10^{-4}	0.9897
$0.5C_{60}$/CZS	0.016	4.1×10^{-4}	0.9951
$1C_{60}$/CZS	0.018	6.5×10^{-4}	0.9916
$2C_{60}$/CZS	0.024	0.0013	0.9854
$5C_{60}$/CZS	0.020	0.002	0.9917

Table 2 Catalytic degradation of Rhodamine B by different catalysts

Photocatalyst	Preparation	Degradation efficiency	k (min^{-1})	References
CdS/g-C_3N_4	Ultrasonic physical mixing	180 min 95%	0.019	[33]
g-C_3N_4/ZnS/CuS	Ultrasonic ultraviolet light wave synthesis	90 min 90%	0.030	[34]
BiOBr	Hydrothermal method	140 min 76.6%	0.018	[35]
TiO_2	Hydrothermal method	140 min 80.4%	0.019	[36]
g-C_3N_4/$Zn_{0.5}Cd_{0.5}S$	Coprecipitation-hydrothermal method	120 min 95.5%	0.028	[37]
$PbMoO_4$	Hydrothermal method	150 min 95%	0.022	[38]
C_{60}/$Zn_{0.5}Cd_{0.5}S$	Hydrothermal method	140 min 97.5%	0.024	This work

correlation coefficient value (R^2) of CZS, $0.5C_{60}$/CZS, $1C_{60}$/CZS, $2C_{60}$/CZS, and $5C_{60}$/CZS are shown in Table 1. Obviously, $2C_{60}$/CZS composite has the highest rate constant. The introduction of C_{60} increases k. The apparent reaction rate of $2C_{60}$/CZS photocatalyst was the highest, which is 3.4 times than that of pure $Cd_{0.5}Zn_{0.5}S$ (0.024 min^{-1} vs. 0.007 min^{-1}) (Fig. 4a). It indicated that medicated C_{60} had the ability to efficiently increase the photocatalytic activity of $Cd_{0.5}Zn_{0.5}S$ photocatalysts. Subsequently, the photocatalytic stability of the $2C_{60}$/CZS photocatalysts was determined for comparison. The catalytic efficiency of the catalyst toward Rh B was essentially unchanged after three cycles, suggesting that the catalyst owned a good cyclic stability (Fig. 4b). In addition, some similar studies on the catalytic degradation of Rh B were sorted out and compared with this study (Table 2).

Mechanisms of the increase of photocatalytic activity and stability

In general, luminous surface absorptivity, surface property, and the efficiency of photo charge separation are the determining factors for the photocatalytic activity. Surface properties are usually expressed in terms of specific surface area. The larger the specific surface area, the better the general catalytic effect. The catalytic efficiency of pure CZS nanocrystals can be improved via C_{60} decoration. As shown in Fig. 3a, the absorption of visible light by C_{60}/CZS nanocomposites saw a small increase. The specific surface area of $2C_{60}$/CZS is only slightly higher than that of CZS (41.3 m^2/g vs. 38.4 m^2/g) (Fig. 5). The specific surface areas of other samples

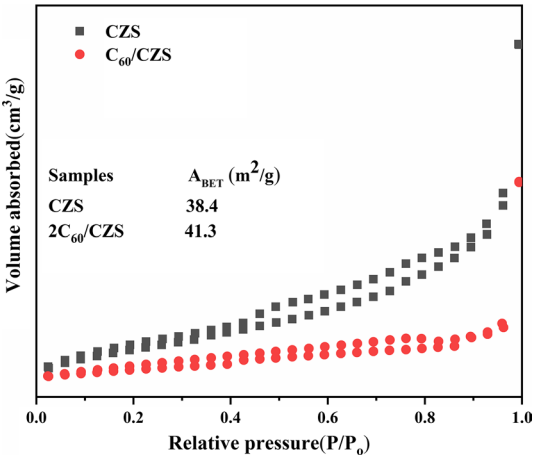

Fig. 5 N_2 adsorption–desorption isotherms in $Cd_{0.5}Zn_{0.5}S$ and $2C_{60}$/CZS samples (the Brunauer–Emmett–Teller surface area was determined by a multipoint BET method using adsorption data in the relative pressure (P/P_0) range of 0.05–0.3)

are 38.6 m^2/g (0.5C_{60}/CZS), 39.6 m^2/g (1C_{60}/CZS) and 41.6 m^2/g (5C_{60}/CZS). Thus, it can be deduced that the effective charge separation and transfer is the leading factor for the high activity, and that the other two factors have little effect.

A photocatalytic mechanism for the composite photocatalyst was made out according to the above experimental results and considering the properties of C_{60}. The VB electrons of CZS semiconductors can be stirred up to the CB after absorbing enough photon energy under visible light irradiation, which makes the VB generate holes (h^+). However, it is inevitable that some photocarriers will recombine quickly and cannot participate in the catalytic reaction. When C_{60} is introduced into the composite system, it can attract photogenerated electrons from the CB of CZS to migrate to the surface, as the CB position of CZS is more negative than that of C_{60} [23]. Thus, the separation of photogenerated electrons and holes on the CZS surface can be effectively enhanced, resulting in more catalytically active species being involved in the catalytic reaction. Besides, the photogenerated holes in the VB of CZS transferred to C_{60} spontaneously, thus preventing the oxidation of CZS by holes. In this experiment, when C_{60}/CZS was used for Rh B photocatalytic degradation, the photogenerated electrons converted the adsorbed O_2 into O_2^- active species, which decomposing Rh B into small molecules. Rh B was also oxidized by photogenerated holes in the VB of CZS [39]. Hence, the C_{60}/CZS composite photocatalyst showed excellent photocatalytic activity and stability.

To further verify the mechanism of enhanced photocatalytic activity and stability, the transient photocurrent response (i−t test) and EIS profiles of $Cd_{0.5}Zn_{0.5}S$ and $2C_{60}$/CZS were recorded. It is known that the photocurrent reflects the separation properties of light-generated electrons and holes. When the photocurrent is high, the separation efficiency would be high. Fig. 6 shows the transient photocurrent response of pure CZS and $2C_{60}$/CZS. The photocurrent density of $Cd_{0.5}Zn_{0.5}S$ was higher compared to $2C_{60}$/CZS, even though the photocurrent of both samples is relatively stable. This suggests that the photogenerated electron–hole separation efficiency is higher in C_{60}/CZS, and more electrons and holes will join the

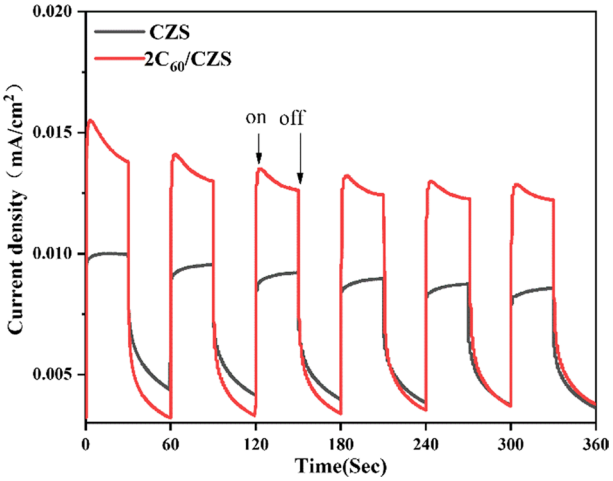

Fig. 6 Transient photocurrent responses of the $Cd_{0.5}Zn_{0.5}S$ and $2C_{60}$/CZS samples (instrument: CHI 660B electrochemical system, test system: standard three-electrode cell system, working electrode: C_{60}/CZS, counter electrode: platinum wire, reference electrode: Ag/AgCl (saturated KCl), electrolyte: 0.1 M Na_2SO_4, radiation source: 300 W xenon lamp coupled with a 420 nm cutoff filter)

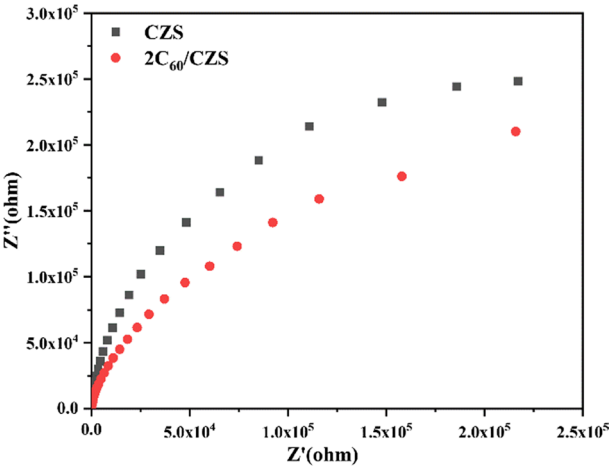

Fig. 7 Nyquist plots of the $Cd_{0.5}Zn_{0.5}S$ and $2C_{60}$/CZS samples (instrument: CHI 660B electrochemical system, test system: standard three-electrode cell system, working electrode: C_{60}/CZS, counter electrode: platinum wire, reference electrode: Ag/AgCl (saturated KCl), electrolyte: 0.1 M Na_2SO_4, radiation source: 300 W xenon lamp coupled with a 420 nm cutoff filter)

catalytic reaction, thus improving the catalytic efficiency. Besides, the EIS results (Fig. 7) also suggested that the C_{60}/CZS system performed better interfacial charge separation and transfer [40]. Accordingly, it was expected that the photocatalytic performance of C_{60}/CZS was better.

Conclusion

In this study, we synthesized $C_{60}/Cd_{0.5}Zn_{0.5}S$ nanocomposites by a facile one-pot hydrothermal preparation method. The degradation efficiency of Rh B was evaluated under visible light irradiation, and the results showed that the catalytic efficiency of C_{60}/CZS was better than that of pure CZS. The optimum content of C_{60} was determined to be 2% when the catalytic efficiency was the highest; the optimal apparent degradation rate of Rh B was 0.024 min^{-1} (degradation efficiency of 97.5%), which is 3.4 times that of the pure CZS reference. Moreover, the cyclic stability of the composites was excellent, and their photocatalytic activity was well maintained after three cycles. The photocurrent measurement and EIS results showed that the introduction of C_{60} can efficiently promote the separation and transfer of photoexcited charge carriers, which in turn can improve the catalytic efficiency. Herein, we innovatively synthesized a novel photocatalyst by combining C_{60} with sulfide solid solution for the first time, which has rarely been studied. Subsequently, the catalytic degradation of Rh B experiment suggested that the catalyst has good catalytic efficiency and stability. This experiment is of great help to the catalytic degradation of Rh B and the application of fullerenes in photocatalysis.

Author contributions All authors contributed to the study conception and design. Material preparation, data collection and analysis were performed by HZ, CD, ZX and JY. The first draft of the manuscript was written by HZ and all authors commented on previous versions of the manuscript. All authors read and approved the final manuscript.

Funding The authors did not receive support from any organization for the submitted work.

Data availability The data that support the findings of this study are available from the corresponding author upon reasonable request.

Declarations

Conflict of interest All authors certify that they have no affiliations with or involvement in any organization or entity with any financial interest or non-financial interest in the subject matter or materials discussed in this manuscript.

References

1. Feng X, Maier S, Salmeron M (2012) Water splits epitaxial graphene and intercalates. J Am Chem Soc 134:5662–5668. https://doi.org/10.1021/ja3003809
2. Hoffmann MR, Martin ST, Choi W, Bahnemann DW (1995) Environmental applications of semiconductor photocatalysis. J Chem Rev 95:69–96. https://doi.org/10.1021/CR00033A004
3. Chen X, Mao SS (2007) Titanium dioxide nanomaterials: synthesis, properties, modifications, and applications. Chem Rev 107:2891–2959. https://doi.org/10.1021/cr0500535
4. Ke D, Liu S, Dai K, Zhou J, Na N, Peng T (2009) CdS/regenerated cellulose nanocomposite films for highly efficient photocatalytic H_2 production under visible light irradiation. J Phys Chem C. https://doi.org/10.1021/jp903378q

5. Kudo A, Miseki Y (2009) Heterogeneous photocatalyst materials for water splitting. Chem Soc Rev 38:253–278. https://doi.org/10.1039/b800489g
6. Iqbal S, Pan Z, Zhou K (2017) Enhanced photocatalytic hydrogen evolution from in situ formation of few-layered MoS_2/CdS nanosheet-based van der Waals heterostructures. Nanoscale 9:6638–6642. https://doi.org/10.1039/c7nr01705g
7. Shi R, Ye HF, Liang F, Wang Z, Li K, Weng Y, Lin Z, Fu WF, Che CM, Chen Y (2018) Interstitial P-doped CdS with long-lived photogenerated electrons for photocatalytic water splitting without sacrificial agents. Adv Mater. https://doi.org/10.1002/adma.201705941
8. Wu J-C, Zheng J, Wu P, Xu R (2011) Study of native defects and transition-metal (Mn, Fe Co, and Ni) doping in a zinc-blende CdS photocatalyst by DFT and hybrid DFT calculations. J Phys Chem C. https://doi.org/10.1021/jp109567c
9. Luo M, Liu Y, Hu J, Liu H, Li J (2012) One-pot synthesis of CdS and Ni-doped CdS hollow spheres with enhanced photocatalytic activity and durability. ACS Appl Mater Interfaces 4:1813–1821. https://doi.org/10.1021/am3000903
10. Zhong W, Huang X, Xu Y, Yu H (2018) One-step facile synthesis and high H_2-evolution activity of suspensible $Cd_xZn_{1-x}S$ nanocrystal photocatalysts in a S^{2-}/SO_3^{2-} system. Nanoscale 10:19418–19426. https://doi.org/10.1039/c8nr06883f
11. Li Q, Meng H-H, Zhou P, Zheng Y, Wang J, Yu J, Gong JR (2013) $ZnO_{1-x}Cd_xS$ solid solutions with controlled bandgap and enhanced visible-light photocatalytic H_2-production activity. J ACS Catal 3:882–889. https://doi.org/10.1021/CS4000975
12. Chen J, Chen J, Li Y (2017) Hollow ZnCdS dodecahedral cages for highly efficient visible-light-driven hydrogen generation. J Mater Chem A. https://doi.org/10.1039/C7TA07587A
13. Yu G, Zhang W, Sun Y, Xie T, Ren A-M, Zhou X, Liu G (2016) A highly active cocatalyst-free semiconductor photocatalyst for visible-light-driven hydrogen evolution: synergistic effect of surface defects and spatial bandgap engineering. J Mater Chem A. https://doi.org/10.1039/C6TA03803D
14. Shen C-C, Liu Y-N, Zhou X, Guo H-L, Zhao Z, Liang K, Xu A-W (2017) High improvement of visible-light photocatalytic H_2-evolution based on cocatalyst-free $Zn_{0.5}Cd_{0.5}S$ synthesized by a two-step process. Catal Sci Technol. https://doi.org/10.1039/C6CY02382G
15. Wu L, Gong J, Ge L, Han C, Fang S, Xin Y, Li Y, Lu Y (2016) AuPd bimetallic nanoparticles decorated $Cd_{0.5}Zn_{0.5}S$ photocatalysts with enhanced visible-light photocatalytic H_2 production activity. Int J Hydrog Energy 41:14704–14712. https://doi.org/10.1016/j.ijhydene.2016.04.157
16. Tang L, Kuai L, Li Y, Li H, Zhou Y, Zou Z (2018) $Zn_xCd_{1-x}S$ tunable band structure-directing photocatalytic activity and selectivity of visible-light reduction of CO_2 into liquid solar fuels. Nanotechnology 29:064003. https://doi.org/10.1088/1361-6528/aaa272
17. Xue W, Chang W, Hu X, Fan J, Liu E (2021) 2D mesoporous ultrathin $Cd_{0.5}Zn_{0.5}S$ nanosheet: fabrication mechanism and application potential for photocatalytic H_2 evolution. Chin J Catal 42:152–163. https://doi.org/10.1016/S1872-2067(20)63593-8
18. Liu T, Li Q, Qiu S, Wang Q, Peng X, Yuan H, Wang X (2020) Construction of $Zn_{0.5}Cd_{0.5}S$ nanosheets and the hybridization with onion-like carbon for enhanced photocatalytic hydrogen production. Appl Surf Sci 525:146586. https://doi.org/10.1016/j.apsusc.2020.146586
19. Peng S, An R, Li Y, Lu G, Li S (2012) Remarkable enhancement of photocatalytic hydrogen evolution over $Cd_{0.5}Zn_{0.5}S$ by bismuth-doping. Int J Hydrog Energy 37:1366–1374. https://doi.org/10.1016/j.ijhydene.2011.09.140
20. Ong W-J, Yeong J-J, Tan L-L, Goh BT, Yong S-T, Chai S-P (2014) Synergistic effect of graphene as a co-catalyst for enhanced daylight-induced photocatalytic activity of $Zn_{0.5}Cd_{0.5}S$ synthesized via an improved one-pot co-precipitation-hydrothermal strategy. RSC Adv 4:59676–59685. https://doi.org/10.1039/C4RA10467F
21. Du H, Xie X, Zhu Q, Lin L, Jiang YF, Yang ZK, Zhou X, Xu AW (2015) Metallic MoO_2 cocatalyst significantly enhances visible-light photocatalytic hydrogen production over $Mo_2/Zn_{0.5}Cd_{0.5}S$ heterojunction. Nanoscale 7:5752–5759. https://doi.org/10.1039/c4nr06949h
22. Lebedeva MA, Chamberlain TW, Khlobystov AN (2015) Harnessing the synergistic and complementary properties of fullerene and transition-metal compounds for nanomaterial applications. Chem Rev 115:11301–11351. https://doi.org/10.1021/acs.chemrev.5b00005
23. Chai B, Liao X, Song F, Zhou H (2014) Fullerene modified C_3N_4 composites with enhanced photocatalytic activity under visible light irradiation. Dalton Trans 43:982–989. https://doi.org/10.1039/c3dt52454j

24. Krätschmer W, Lamb LD, Fostiropoulos K, Huffman DR (1990) Solid C_{60}: a new form of carbon. Nature 347:354–358. https://doi.org/10.1038/347354a0
25. Qi K, Selvaraj R, Al Fahdi T, Al-Kindy S, Kim Y, Wang G-C, Tai C-W, Sillanpää M (2016) Enhanced photocatalytic activity of anatase-TiO_2 nanoparticles by fullerene modification: a theoretical and experimental study. Appl Surf Sci 387:750–758. https://doi.org/10.1016/j.apsusc.2016.06.134
26. Guo W, Tian Y, Jiang L (2013) Asymmetric ion transport through ion-channel-mimetic solid-state nanopores. Acc Chem Res 46:2834–2846. https://doi.org/10.1021/ar400024p
27. Zhu S, Xu T, Fu H, Zhao J, Zhu Y (2007) Synergetic effect of Bi_2WO_6 photocatalyst with C_{60} and enhanced photoactivity under visible irradiation. Environ Sci Technol 41:6234–6239. https://doi.org/10.1021/es070953y
28. Wang S, Liu C, Dai K, Cai P, Chen H, Yang C, Huang Q (2015) Fullerene C_{70}–TiO_2 hybrids with enhanced photocatalytic activity under visible light irradiation. J Mater Chem A 3:21090–21098. https://doi.org/10.1039/C5TA03229F
29. Lente G (2015) Deterministic kinetics in chemistry and system biology: the dynamics of complex reaction networks. Springer, Berlin
30. Yu J, Ma T, Liu G, Cheng B (2011) Enhanced photocatalytic activity of bimodal mesoporous titania powders by C_{60} modification. Dalton Trans 40:6635–6644. https://doi.org/10.1039/c1dt10274e
31. Sahoo PP, Maggard PA (2013) Crystal chemistry, band engineering, and photocatalytic activity of the $LiNb_3O_8$-$CuNb_3O_8$ solid solution. Inorg Chem 52:4443–4450. https://doi.org/10.1021/ic302649s
32. Ge L, Liu J (2011) Efficient visible light-induced photocatalytic degradation of methyl orange by QDs sensitized CdS-Bi_2WO_6. Appl Catal B 105:289–297. https://doi.org/10.1016/j.apcatb.2011.04.016
33. Xu Y, Zhang W-D (2015) CdS/g-C_3N_4 hybrids with improved photostability and visible light photocatalytic activity. Eur J Inorg Chem 10:1744–1751. https://doi.org/10.1002/ejic.201403193
34. Sun Y-J, Jiang J-Z, Cao Y, Liu Y, Wu S-L, Zou J (2018) Facile fabrication of g-C_3N_4/ZnS/CuS heterojunctions with enhanced photocatalytic performances and photoconduction. Mater Lett 212:288–291. https://doi.org/10.1016/j.matlet.2017.10.111
35. Chen A, Zhang J, Zhou Y, Tang H-Q (2021) Preparation of a zinc-based metal-organicframework (MOF-5)/BiOBr heterojunction for photodegradation of Rhodamine B. Reac Kinet Mech Cat 134:1003–1015. https://doi.org/10.1007/s11144-021-02107-4
36. Premalatha N, Rajalakshmi P, Miranda LR (2022) Photocatalytic degradation of Rhodamine B over TiO_2/g-C_3N_4 and immobilized TiO_2/g-C_3N_4 on stainless steel wire gauze under UV and visible light: a detailed kinetic analysis and mechanism of degradation. Reac Kinet Mech Cat. https://doi.org/10.1007/s11144-022-02154-5
37. Martínez-de la Cruz A, Hernández-Uresti DB, Torres-Martínez LM et al (2012) Photocatalyticproperties of $PbMoO_4$ synthesized by a hydrothermal reaction. Reac Kinet Mech Cat 107:467–475. https://doi.org/10.1007/s11144-012-0482-9
38. Qi S-Y, Wang D-P, Zhao Y-D, Xu H-Y (2019) Core-shell g-C_3N_4@$Zn_{0.5}Cd_{0.5}S$ heterojunction photocatalysts with high photocatalytic activity for the degradation of organic dyes. J Mater Sci: Mater Electron 30:5284–5296. https://doi.org/10.1007/s10854-019-00828-w
39. Li Q, Li X, Wageh S, Al-Ghamdi A, Yu J (2015) CdS/graphene nanocomposite photocatalysts. Adv Eng Mater. https://doi.org/10.1002/aenm.201500010
40. Hu Z, Liu G, Chen X-Q, Shen Z, Yu J (2016) Enhancing charge separation in metallic photocatalysts: a case study of the conducting molybdenum dioxide. Adv Funct Mater. https://doi.org/10.1002/adfm.201600239